

Article

# Flow Characteristics of Steam and Gas Push in the Presence of Heat Thief Zones Overlying Oil Sands Deposits

Changsoo Lee, Changhyup Park \*  and Soobin Park

Department of Energy and Resources Engineering, Kangwon National University, Chuncheon, Kangwon 24341, Korea; changsoolee@kangwon.ac.kr (C.L.); soobin.park@kangwon.ac.kr (S.P.)

\* Correspondence: changhyup@kangwon.ac.kr; Tel.: +82-33-250-6259

Received: 19 July 2017; Accepted: 6 September 2017; Published: 7 September 2017

**Abstract:** This paper presents the effects of the top water-bearing zone on the performance of the steam and gas push, i.e., nitrogen as a non-condensable gas injected with steam into an oil sands deposit. The flow characteristics of fluid mixtures are examined in the presence of different-sized water-bearing formations overlying oil sands deposits, i.e., a finite aquifer with no-flow boundaries and an infinite aquifer with continuous mass flux. The performance efficiency is investigated by respectively implementing the cumulative steam to oil ratio, a simple thermal efficiency parameter, and the oil production on the surface. The top water-bearing area serves as a heat thief zone and negatively impacts bitumen recovery; furthermore, it increases the cumulative steam to oil ratio while decreasing the simple thermal efficiency parameter, as well as the oil production rate. When the steam chamber encounters the top aquifer, a severe heat loss occurs. As increasing mol % of nitrogen, the producing time with energy efficiency increases but the chamber growth is limited. The specific operational conditions would be possible for the finite-sized aquifer, while the continuous water influx and the significant heat loss obstructs the thermal processes for the infinite aquifer.

**Keywords:** steam and gas push; non condensable gas; thief zone; thermal efficiency; oil sands; aquifer

## 1. Introduction

Steam-assisted gravity drainage (SAGD), one of the thermal operations for the recovery of extremely viscous oil, releases steam into the native bitumen formation and simultaneously produces the diluted fluid mixture via a production well. A steam chamber, i.e., a steam saturated zone, should grow vertically and spread laterally to obtain the effective gravitational force for successful SAGD operations [1–6]. Impermeable caprock provides the lateral flow by blocking the vertical movement of the fluid mixture, and also to enlarge steam chambers at thin payzones. A significant amount of bitumen reserves comprises negligible caprock with a top water-bearing zone, e.g., oil sands reservoirs in the Surmont leases, Kearsy Lake, and the Wabiskaw-McMurray formation [7–9].

The top water-bearing zone near a native bitumen deposit, typically called a heat thief zone, can be problematic since it reduces the energy efficiency of thermal processes, or it interrupts the growth of the steam chamber due to a water influx or steam loss. Compared with the gas-bearing zone underlying or overlying the oil sands formation, the impact of the top water-bearing area on the energy efficiency, whereby a significant water influx into the reservoir and heat loss from the aquifer occur, is significant [10,11].

To isolate the top water-bearing zone with the oil sands deposit, the steam and gas push (SAGP) that injects non-condensable gas with SAGD operation has been proposed [12–21]. The non-condensable gas, e.g., carbon dioxide, nitrogen, and methane, remains as a gas phase within the steam chamber, is accumulated near the board of the steam chamber, and serves as a screen to

isolate the human-made steam chamber from the thief zone. However, as the screen is thicker, the growth of the steam chamber is restricted, meaning that the energy efficiency of the thermal process can be reduced even when the blocking effect increases. The non-condensable gas obstructs the heat of the steam from passing through the native bitumen and, consequently, the inclined edges of the steam chamber fail to generate the gravitational forces that draw the optimum downward flow to the producer. An improper high fluid injection can result in a severe steam loss, while the lower pressure within the steam chamber would cause a water invasion from the top aquifer, leading to a significant reduction of the temperature within the steam chamber, thereby resulting in the failure of the enhanced bitumen recovery. A numerical simulation of the steam and non-condensable gas, e.g., nitrogen, push without the top water-bearing area showed that the gas conserved the heat of the steam chamber to accomplish the desired economics [17]. If a fixed-size aquifer exists, another numerical analysis showed that the nitrogen in the SAGD process could improve the oil productivity [19,20]. The focus of the previous works is the formulation of a way to accomplish energy efficiency during the performance of the thermal operation to overcome the top water zone. The fixed-size thief zone surrounded by a no flow formation, e.g., a lens-shaped water zone, has been researched, and some of the problematic effects of non-condensable gas could be overlooked, such as the aquifer sizes.

This study analyzes the possibility regarding the use of co-injected nitrogen as a non-condensable gas to overcome the problematic effects of the top water-bearing thief zone. The influence of the aquifer size is investigated in terms of its effect on the SAGD process. Two boundary conditions are evaluated as follows: the finite no-flow boundary and the continuous mass flux. To achieve field applicability, several constraints regarding the well operation are considered, i.e., the injected amount of nitrogen and the operation conditions at a production well (bottom hole pressure, surface liquid rate, and steam rate).

## 2. Methodology

A synthetic reservoir model is constructed with the typical properties of the oil sands reservoirs in Athabasca, AB, Canada. The 2D homogeneous reservoir is assumed to eliminate the effects of mass transfer along to the direction of horizontal well, i.e., the  $j$  direction, and also those of heterogeneous rock properties affecting the fluid flow between the water-bearing zone and the oil sands deposit. Table 1 summarizes the reservoir properties and Table 2 shows the molecular weight and viscosities of the oil with temperature. The molecular weight of nitrogen is 28.013 kg/kg-mol. The critical pressure and temperature of nitrogen are 3394 kPa and  $-146.95$  °C (degrees Celsius). The solubility of nitrogen in liquid is assumed that its value is small enough to be ignored. The effect of solution gas dissolved in oil is neglected so that the gas phases are assumed as steam and nitrogen. The gas-liquid  $K$  value of nitrogen is assumed as a function of pressure and temperature (see Equation (1)).

$$K = \frac{a}{P} \exp\left(\frac{b}{T - c}\right) \quad (1)$$

In Equation (1),  $K$  denotes the  $K$  value of nitrogen.  $P$  represents the pressure (kPa) and  $T$  is temperature (°C). The coefficients  $a$ ,  $b$ , and  $c$  are 416,360,  $-588.72$ , and  $-266.55$ , respectively. The mole fraction (mol %) of the injected-steam amount determines the nitrogen volume. The temperatures of the steam and nitrogen are both 250 °C. The horizontal permeability ( $i$  and  $j$  directions; lateral direction) is 2.5 Darcy, and the vertical permeability is 1.25 Darcy.

**Table 1.** Input properties used in the synthetic reservoir model. TVD: true vertical depth.

Geological Parameter	Value
Initial reservoir temperature (°C)	12
Initial reservoir pressure at 240 mTVD (kPa)	1600
Horizontal absolute permeability (Darcy)	2.5
Vertical absolute permeability (Darcy)	1.25
Porosity (–)	0.3
Initial oil saturation of the payzone (–)	0.8
Irreducible water saturation (–)	0.2
Rock volumetric heat capacity (kJ/m <sup>3</sup> ·°C)	2600
Rock thermal conductivity (kJ/m·day·°C)	660
Gas thermal conductivity (kJ/m·day·°C)	5
Oil thermal conductivity (kJ/m·day·°C)	11.5
Water thermal conductivity (kJ/m·day·°C)	53.5

**Table 2.** Properties of the oleic component.

Property	Value
Oil molecular weight (kg/kg-mol)	570
Oil viscosity at 10 °C (cp)	2,864,376
Oil viscosity at 90 °C (cp)	655
Oil viscosity at 250 °C (cp)	6

Table 3 shows the operational constraints of the SAGP process. Figure 1 depicts the top water-bearing zones and an oil sands deposit, wherein Figure 1a shows a finite aquifer, and Figure 1b illustrates an infinite aquifer. The upper area of both aquifers is assumed as impermeable. One injector is installed at 255 mTVD (true vertical depth), and a producer is located at 5 m below the injector. The vertical thickness of the bitumen formation is 15 m, and that of the top water-bearing zone is 13 m. The horizontal distance of the bitumen layer is 123 m. The grid system of the bitumen layer is rectangular; the grid size comprises  $(\Delta i, \Delta j, \Delta k) = (1 \text{ m}, 20 \text{ m}, 0.5 \text{ m})$ , and its grid number is  $(N_i, N_j, N_k) = (123, 1, 30)$ . Both of the formation-volume factors of the oil and water are assumed as 1. The stock tank oil initially in place (*STOIIP*) is calculated as 8821.8 m<sup>3</sup>.

The grid organizations of the finite aquifer (see Figure 1a) are  $(\Delta i, \Delta j, \Delta k) = (1 \text{ m}, 20 \text{ m}, 1.3 \text{ m})$  and  $(N_i, N_j, N_k) = (123, 1, 10)$ . In the infinite aquifer, the aquifer size is increased so that its grid numbers are  $(N_i, N_j, N_k) = (137, 1, 10)$  (see Figure 1b). To demonstrate the constant pressure boundaries and the continuous mass transfer in the infinite aquifer, four image wells are located at the edges of the aquifer boundaries, as illustrated in Figure 1b. In consideration of the gravity force, the pressures of the image wells are set as 1524 kPa for the injector and 1528 kPa for the producer to prevent a natural downward flow. The SAGP is modeled using the thermal simulator, STARS (Computer Modelling Group, Calgary, AB, Canada) [22]. The following three parameters are implemented to evaluate the energy efficiency of the SAGP operation: steam to oil ratio (*SOR*; Equation (2)), cumulative steam to oil ratio (*cSOR*; Equation (3)), and simple thermal efficiency parameter (*STEP*; Equation (4)).

$$SOR = \frac{V_{s,t}}{V_{o,t}} \quad (2)$$

$$cSOR = \frac{\sum_{t=0}^n V_{s,t}}{\sum_{t=0}^n V_{o,t}} \quad (3)$$

**Table 3.** Well constraints for the steam and gas push (SAGP) modeling.

Well Type	Constraints	Condition	Value
Injector	Surface total phase rate (m <sup>3</sup> /day CWE) <sup>1</sup>	Maximum	6.0
Producer	Bottom hole pressure (kPa)	Minimum	1300
	Surface liquid rate (m <sup>3</sup> /day)	Maximum	7.5
	Steam rate (m <sup>3</sup> /day)	Maximum	0.2

<sup>1</sup> Surface total phase rate means the total volume from the summation of the injection rates of both the steam and the nitrogen (non-condensable gas). CWE stands for “cold-water equivalent”.

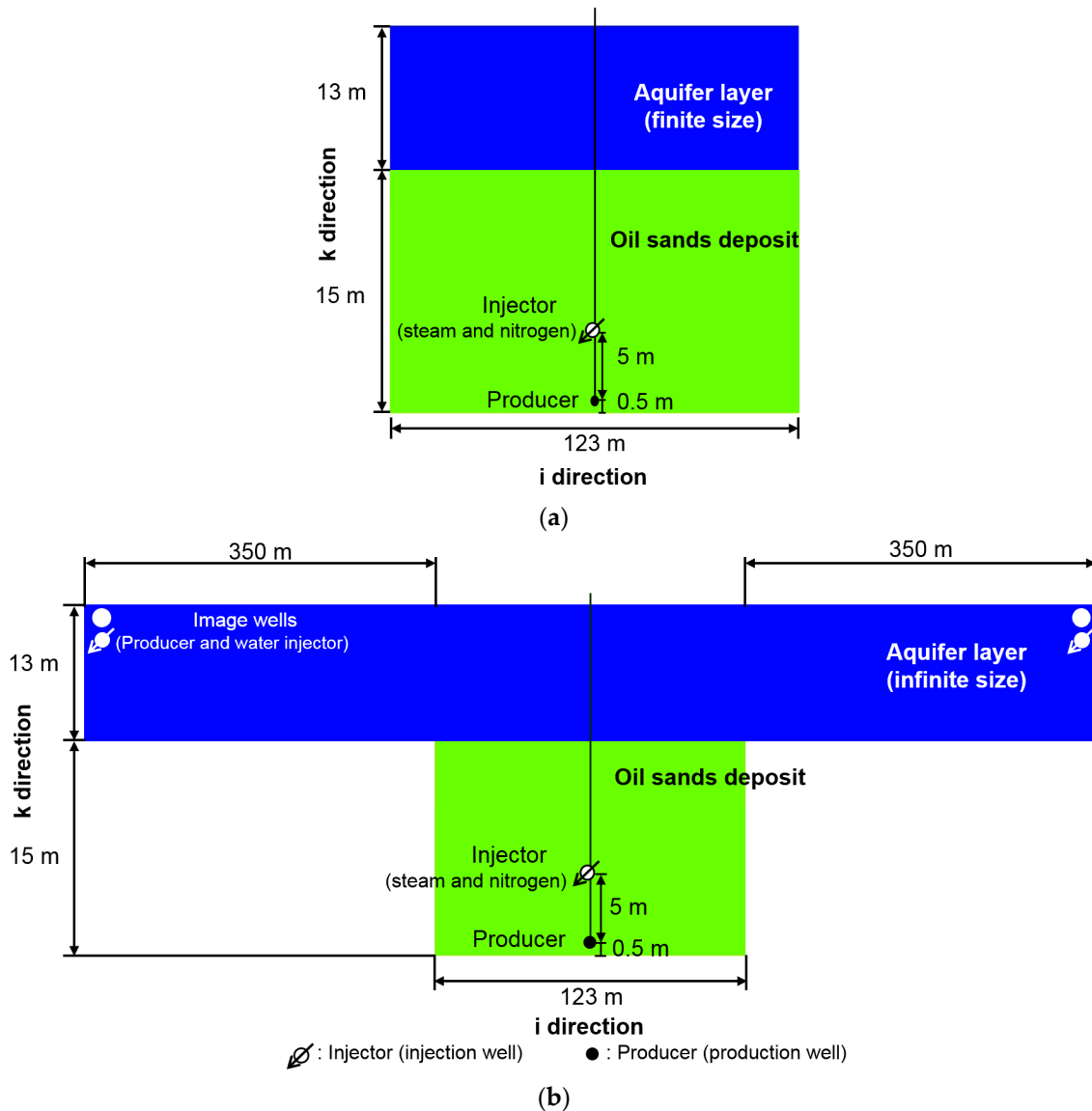


**Figure 1.** Schematic diagram of the synthetic models including: (a) the finite aquifer; and (b) the infinite aquifer.

In Equations (2) and (3),  $V$  is the volume, and the subscripts  $s$  and  $o$  represent the injected steam and the produced oil, respectively, i.e.,  $V_{o,t}$  is the oil production rate at time  $t$ . In this study, the daily rates at the injector and the producer are used.  $n$  indicates the end of the SAGP process.  $STEP$  has

been developed to examine the optimum energy-efficient operations that show the highest recovery, as defined in Equation (4) [23]:

$$STEP = \frac{(RF/0.5) \times (CDOR/0.111)}{(cSOR/3)^{2.4}} \quad (4)$$

$$CDOR = \frac{\frac{1}{n} \sum_{t=0}^n V_{o,t}}{L_h} \quad (5)$$

$$RF = \frac{\sum_{t=0}^n V_{o,t}}{STOIPP} \quad (6)$$

In Equations (4)–(6), *CDOR* stands for the “calendar day oil rate”, which is the average oil production rate per unit of perforated length, i.e., the average value of the daily production rate divided by the total perforated length ( $L_h$ ). This study assumes a full perforation along with horizontal wells and  $L_h$  is, therefore, equal to  $\Delta j$  (=20 m). *RF* represents the “recovery factor” that is calculated using *STOIPP* (=8821.8 m<sup>3</sup>) and the cumulative volume of the produced oil. The figures that serve as the denominators in Equation (3) are the abandonment values per each parameter that are obtained from the commercial field database of an actual oil sands development, as follows: 0.5 for *RF*, 0.111 for *CDOR*, and 3 for *cSOR*. The exponent of 2.4 in Equation (3) is determined to show a linear relationship with the net present value when the steam cost is \$5/barrel and the bitumen commodity price is \$20/barrel [23].

### 3. Results and Discussion

#### 3.1. Effects of Boundary Condition of the Top Water-Bearing Zone

The SAGP simulation is carried out assuming 1 mol % of nitrogen, i.e., the SAGD operation injecting the nitrogen of which mole fraction to the steam amount is 1 mol %. The presence of the top water-bearing zone not only decreases the thermal efficiency, but also the oil productivity, regardless of the aquifer type. The performances of the SAGP process at the finite boundaries are more effective than those of the infinite case (refer to Figure 2). Figure 2 describes the production performances in accordance with the aquifer type, as follows: Figure 2a shows the trends of the oil production rate and Figure 2b depicts the water cut, i.e., the ratio of water produced compared to the volume of total liquids produced in the production well. Prior to the encounter between the steam chamber and the water-bearing thief zone, all of the performances are the same regardless of the boundary conditions; however, after the aquifer provides the effects on the chamber enlargement, different performances are observed according to the aquifer type. The oil sands deposit with the finite-sized water-bearing thief zone produces more oil and less water compared with the infinite condition. The water production increases by meeting the top water-bearing zone around 200 days, but the difference in oil production rates is not large, as shown in Figure 2b. After about 320 days, the significant decrement of the oil rate is observed, due to the boundary effect (see Figure 2a); furthermore, the water cut increases by supplying the groundwater for the case of infinite aquifer while, in the finite aquifer, the water is replaced with the injected fluids and thereby the trend of the decreasing oil production rate is slower than that of the finite-sized thief zone. The fluctuation from 300 days to 400 days, in the case of the infinite aquifer, explains a transient change, whereby the accumulation of the high pressure in the steam chamber does not respond to long-distance pressure boundaries. In the case of the infinite aquifer, it might take time to arrive at the equilibrium state. The detailed analyses related to the liquid production reveal that the infinite aquifer incurs more-problematic effects by continuously supplying a larger water influx amount. Since this simulation maintains a constant liquid production and injection

volume, as shown in Table 3, the trajectories of the daily water cut can analogize the amount of the water influx from the top water-bearing zone.

Figure 3 depicts the parameters related to the examination of energy (thermal) efficiency; the observations of the *SOR* (Figure 3a), the *cSOR* (Figure 3b), and the *STEP* (Figure 3c), respectively. The smaller the *SOR* and the *cSOR*, and the larger *STEP*, the more efficient the method of thermal process. Figure 3a shows that the *SOR* is sharply increased near 400 days and the slope of the *SOR* in the finite aquifer is smaller. At that time, the *SOR* value is about 8, whereby it would be assumed that the SAGP operation with negligible effects of aquifer has been until the *SOR* reaches 8, i.e., the *cSOR* is around 4 in Figure 3b. Figure 3c confirms that the SAGP in the presence of finite-sized heat thief zone is more profitable and more efficient than those of infinite case; furthermore, the finite aquifer shows the higher *STEP*, as well as the longer arrival time at the maximum value.

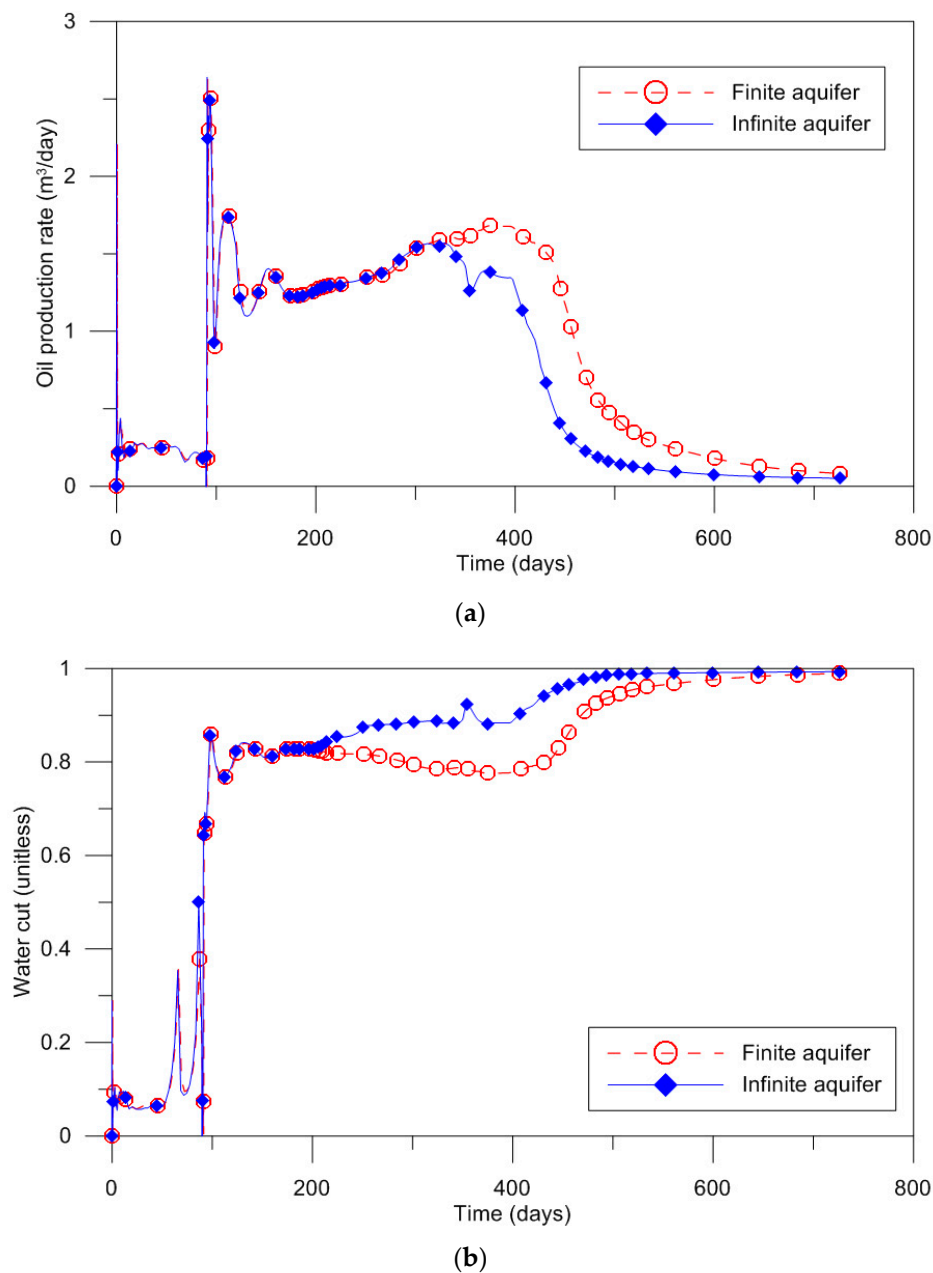


**Figure 2.** Comparison of liquid production performances with time: (a) oil production rate; and (b) water cut.

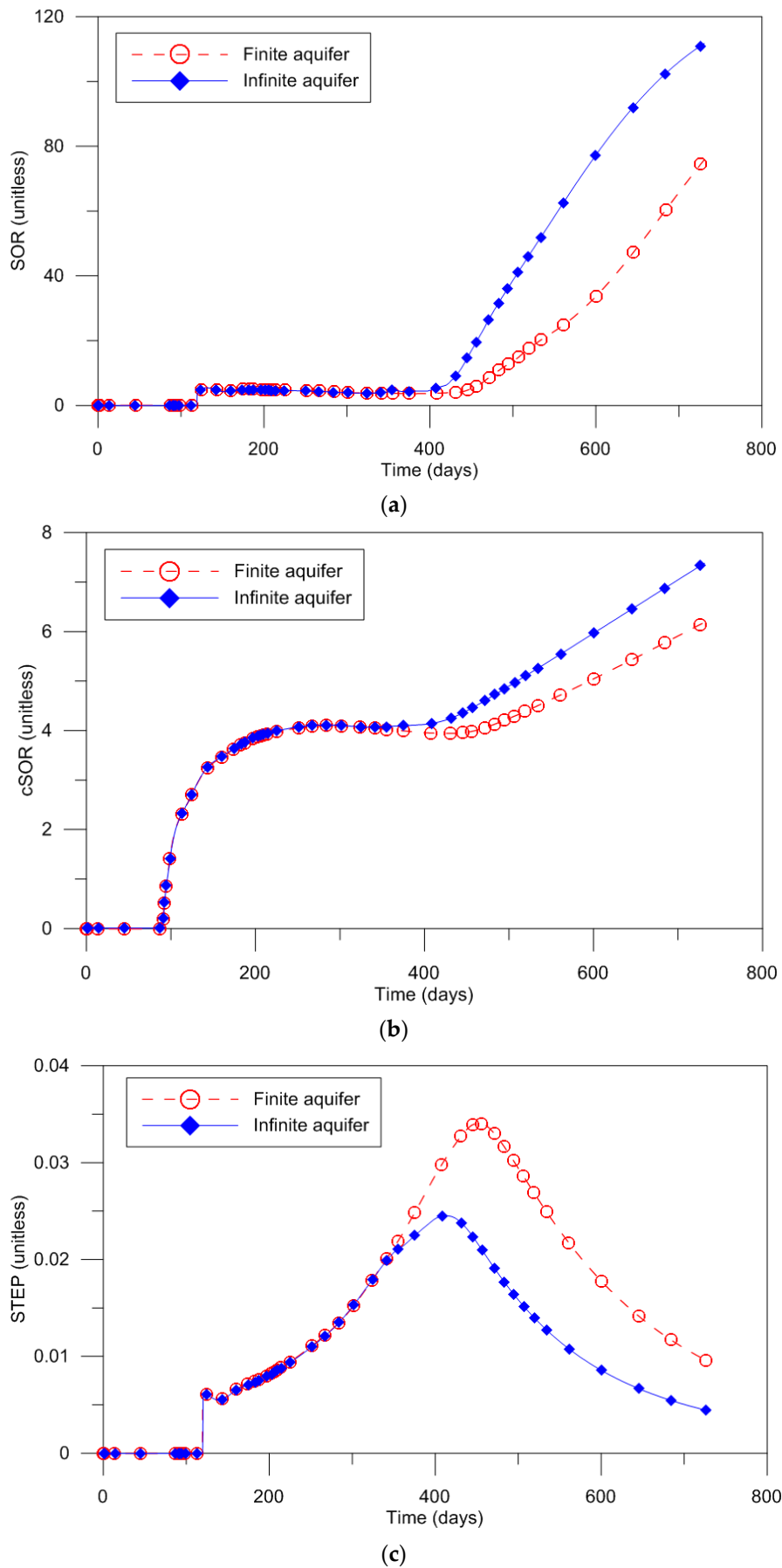


**Figure 3.** Comparison of energy efficiency with time: (a) steam to oil ratio (SOR); (b) cumulative steam to oil ratio (cSOR); and (c) simple thermal efficiency parameter (STEP).

The flow characteristics of steam and nitrogen within the reservoir evaluate the effects of the nitrogen regarding the preservation of the proper growth of the steam chamber. Figure 4 illustrates the percentage of nitrogen regarding the gas (united steam and nitrogen) saturation at the end of the SAGP process (two years from the first oil), wherein the saturation distribution of the finite case (see Figure 4a) is compared with that of the infinite aquifer (see Figure 4b). For example, 40% nitrogen concentration means that 40% of nitrogen and 60% of steam comprise the gas volume in the grid cell since there is no gas phase except for nitrogen and steam. The nitrogen distribution shows the advantage of the non-condensable gas whereby it maintains the steam chamber, and in the finite aquifer, the screen of nitrogen is well developed by accumulating near the steam chamber edges. In the middle of steam chamber, the water influx could be unavoidable and thereby it reduces the energy efficiency and interrupts the desired chamber growth. At the same time of the water influx, the severe gas loss, especially the nitrogen, into the aquifer is observed.

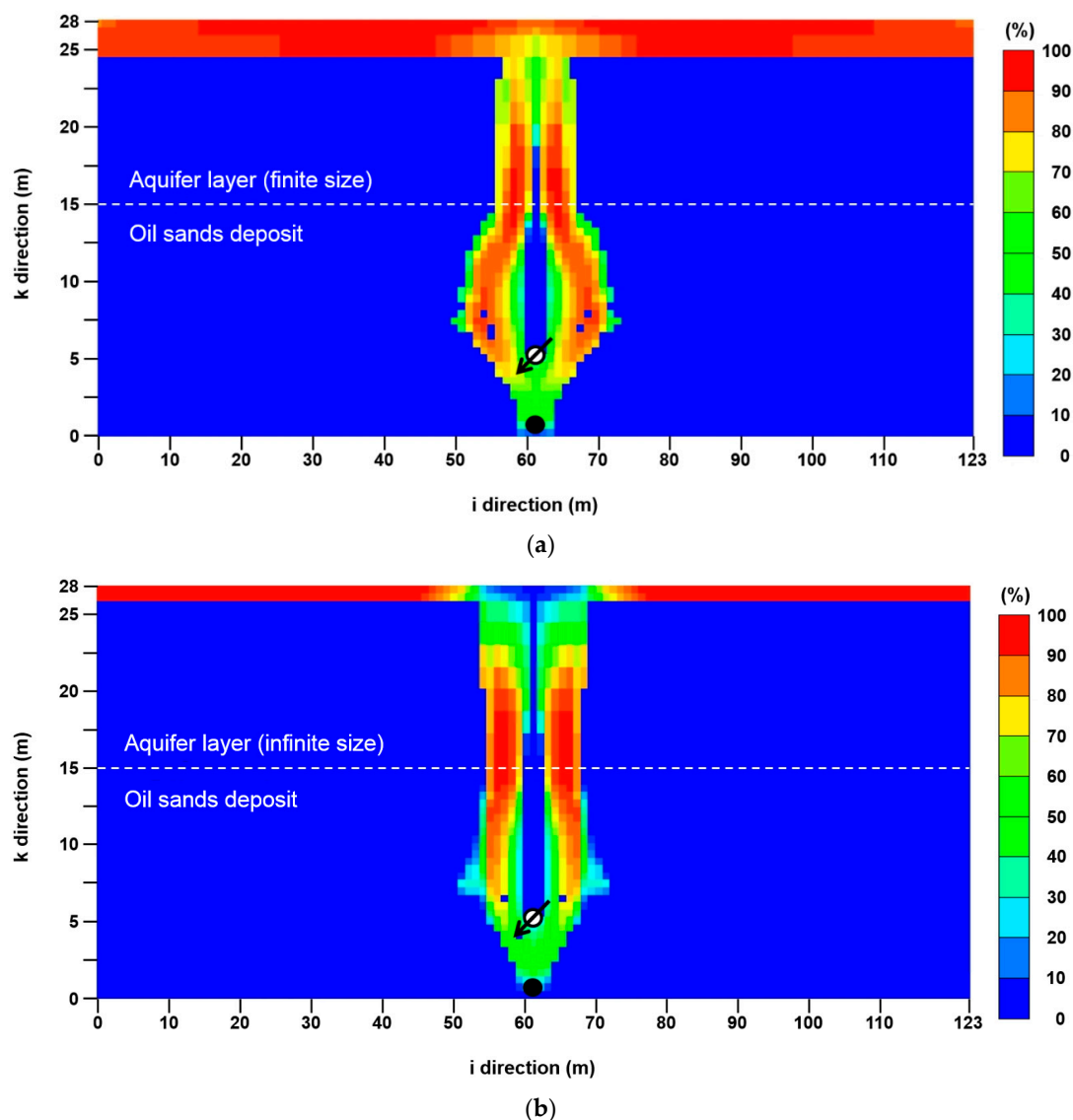


**Figure 4.** Nitrogen concentration to gas saturation at the end of production in the cases of: (a) the finite aquifer; and (b) the infinite aquifer.

The injected fluid mixture, i.e., steam and nitrogen, moves vertically to the top aquifer and then spreads sideways due to the no-flow conditions at the upper area of the top aquifer. The released

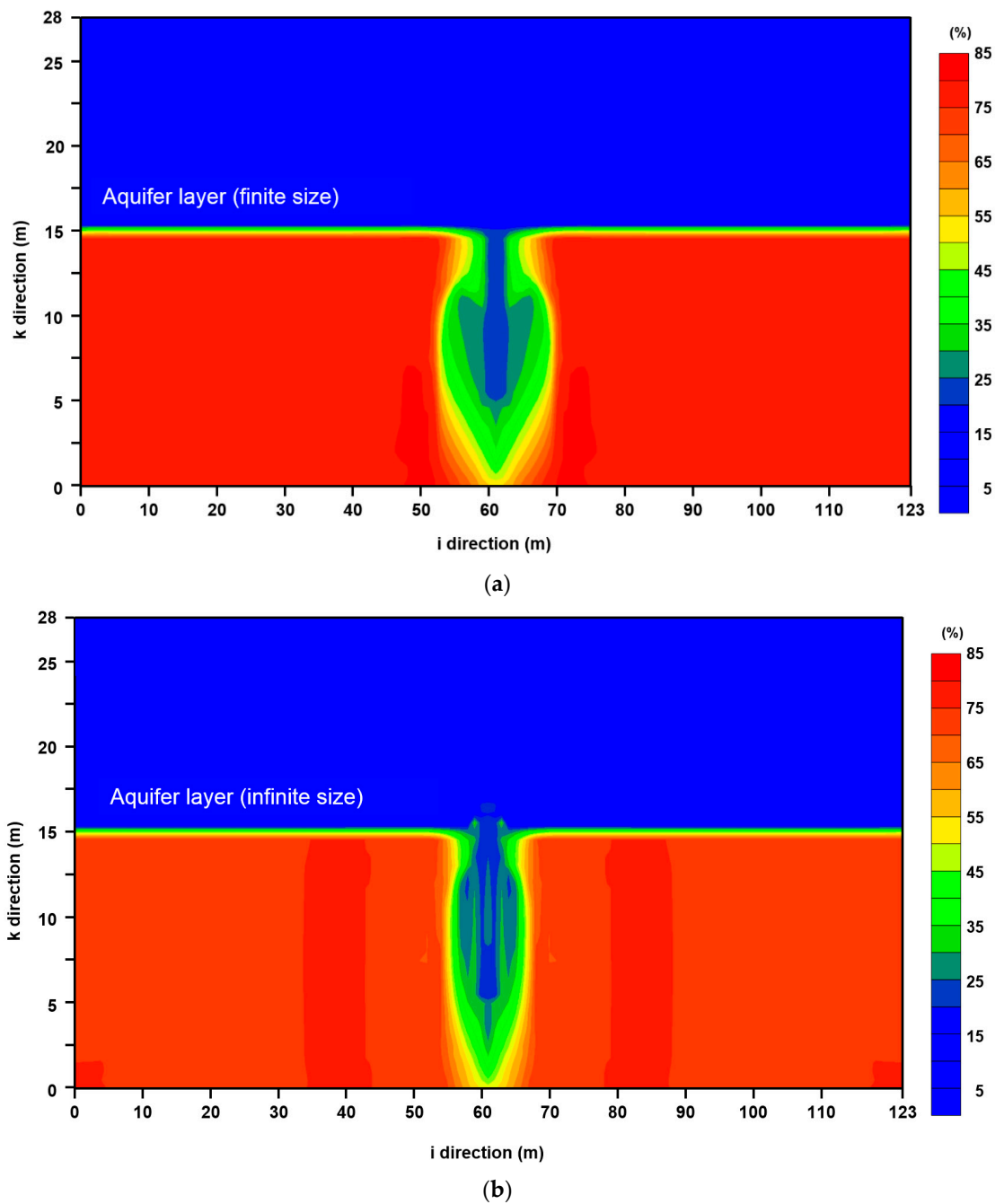
mass (gas movement from the steam chamber into the aquifer) increases the formation pressure of the aquifer so that the formation water is expelled to the lateral direction or it flows downward. The gas loss into the thief zone and the water influx into the steam chamber can occur simultaneously. All of the gas phases gather near the upper no-flow boundaries of the aquifer and spread sideways. As a result of the no-flow occurring on either side of the finite aquifer, the lateral movement of the fluids is limited regarding the formation water in the aquifer, and the steam is able to move to the steam chamber.

Figure 5 describes oil saturation at the end of SAGP operation; Figure 5a shows the case of the finite aquifer and Figure 5b shows that of infinite case. This result represents how well the steam chamber can develop laterally; Figure 5a shows that the lateral growth of steam chamber is possible, notwithstanding that the water influx occurs in the middle of steam chamber, while Figure 5b explains that the thermal operation is unavailable due to dominant vertical flow and ineffective lateral flow, i.e., horizontal enlargement. The infinite aquifer provides continuous water influx with low temperature into the oil sands deposit and the steam chamber, and the gas phase with high temperature leaks out. These flow characteristics show the difficulties to develop the desired shape of the steam chamber, to maintain the chamber, and to enlarge the chamber in the horizontal direction without heat thief zones.

These results can explain the transport of the steam and nitrogen that occurred during SAGP operation; furthermore, it can also support the production performances of Figures 2 and 3, whereby the finite case shows a higher energy efficiency and oil recovery. At the fixed-size water-bearing area, the objectives of the nitrogen injection can be achieved, since the injected nitrogen releases into the aquifer and forms a screen to prevent the water influx; however, a significant nitrogen loss is unavoidable, and the achievement of the desired efficiency is, consequently, difficult.

The most important condition can be the determination of the optimal operations for the prevention of both the water influx and the heat loss. The unequal distribution of pressures in the steam chamber induces the co-occurrence of the water invasion into the steam chamber and the heat loss into the aquifer, as shown in Figure 4. If the fluids, i.e., steam and nitrogen, are injected with a higher pressure, the vertical growth of the steam chamber is dominant, and the steam chamber meets the aquifer at an early time as a result. The steam chamber encounters the aquifer at an early time so that the heat loss is significant. Overall, this significant water influx stops the chamber growth and impedes the heat preservation in the chamber. Alternatively, a lower pressure delays the chamber enlargement, interrupts the transmission of the latent heat to the formation, and decreases the energy efficiency. The operational constraints at the production well can be used to determine the length of time the latent heat stays in the chamber. If the mobilized hydrocarbon is produced at a slow speed, the chamber temperature decreases little by little before crossing over the aquifer, but the water influx reduces the temperature quickly so that the heat balance will be broken. The infinite boundaries can provide a continuous water influx and heat loss so that the favorable effects of the nitrogen for the preservation of the well-developed steam chamber are negligible. As the steam replaces the top water in the finite case, the energy loss could be overcome, but the expectation that the favorable effect will prevent the heat loss as the size of the top water-bearing area increases is unrealistic.

To briefly conclude, notwithstanding the operators' hope of running the SAGP in a manner similar to the low-pressure SAGD (LP-SAGD), the determination of the optimum injection is a far-reaching challenge. It is challenging to demonstrate the boundary conditions that are required for a real aquifer overlying oil sands formations. As shown in the above results, the setting-up of the boundaries and the image wells can affect the entire performance of the SAGP process. If higher bottom hole pressures are applied at the image wells, it is possible that a more severe water influx would be observed entering the steam chamber.

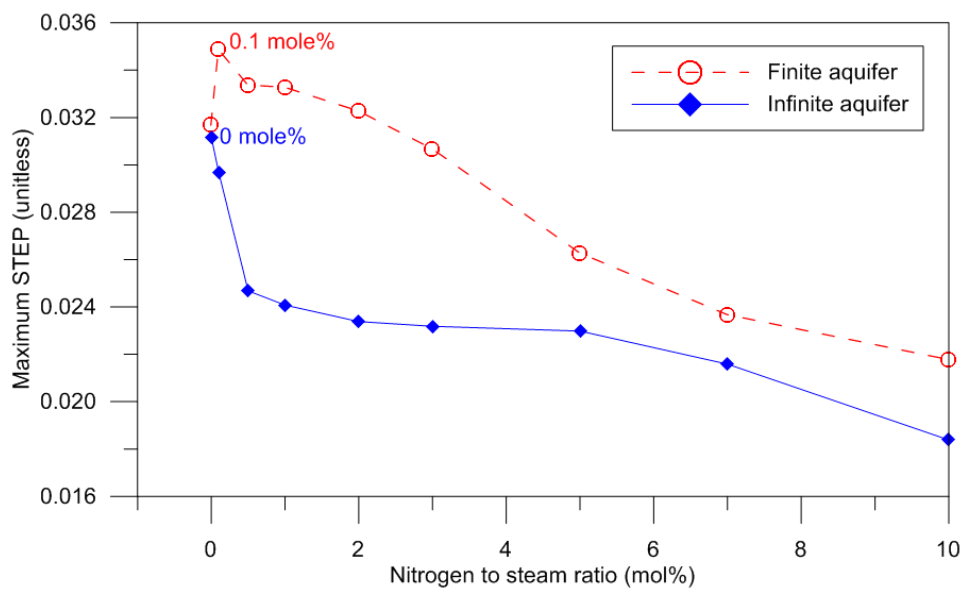


**Figure 5.** Oil saturation at the end of production in the cases of: (a) the finite aquifer; and (b) the infinite aquifer.

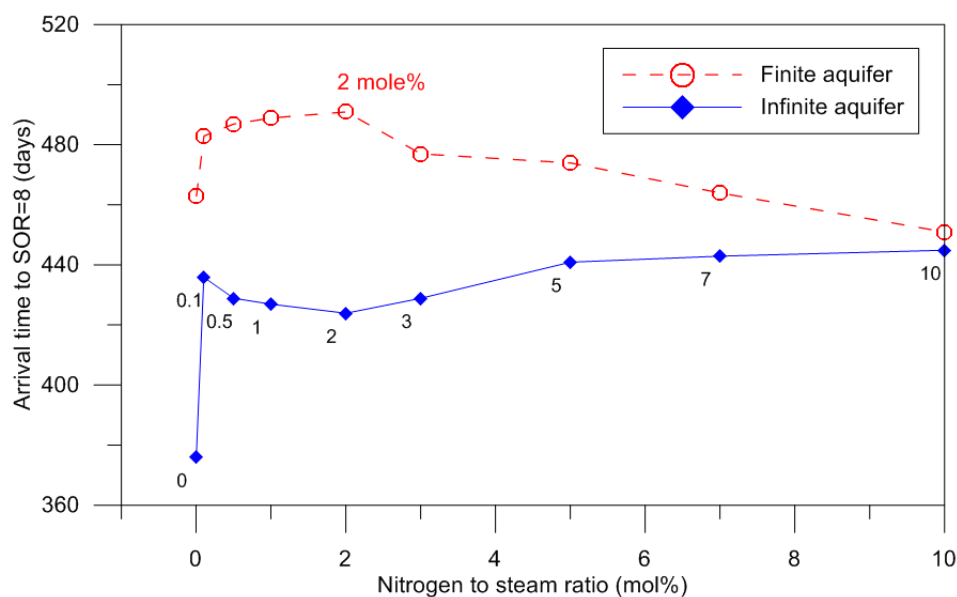
### 3.2. Effects of the Nitrogen Volume

The maximum *STEP* values and the producible period with energy efficiency are observed from the changing of the mole fraction of the nitrogen from 0 mol % to 10 mol %. Nine cases were examined, as follows: 0 mol %, 0.1 mol %, 0.5 mol %, 1 mol %, 2 mol %, 3 mol %, 5 mol %, 7 mol %, and 10 mol %. As demonstrated in Figure 3c, the *STEP* value increases and then decreases due to the problematic effects of the top water-bearing thief zone. The maximum value here, obtained at an inflection point of the Figure 3c curve, represents the maximum profitable point with energy efficiency. Figure 6 shows, according to the nitrogen concentration, the maximum *STEP* and the arrival time when *SOR* is 8, i.e., the inflection point in Figure 3a that means the producible period with energy efficiency; Figure 6a

draws the maximum *STEP* and Figure 6b shows the arrival time to *SOR* = 8. Table 4 summarizes these results with the maximum values. Figure 6a confirms that the optimum nitrogen mole fraction is 0.1 mol % in the finite aquifer, while SAGD without nitrogen injection is most efficient in the case of the infinite aquifer with continuous mass flux. Since significant and continuous water influx into the steam chamber is unavoidable, if we have the infinite aquifer overlying the oil sands reservoir, the fast thermal process would be desirable until the chamber arrives at the top water-bearing zone, shutting in the wells, and then a new infill drilling would be an alternative. If the operators want to the larger producible time, 2 mol % of nitrogen would be a solution in the finite aquifer. For the case of the infinite aquifer, Figure 6b would suggest the large amount of nitrogen injection, but the nitrogen interrupts the chamber growth and thereby results in ineffective SAGP operation.



(a)



(b)

**Figure 6.** Effects of the nitrogen mole fraction on *STEP* and the production time with energy efficiency: plot of (a) the maximum *STEP* and (b) the arrival time to *SOR* = 8 vs. the nitrogen to steam ratio at the injector.

**Table 4.** Summary of the nitrogen mole fraction affecting the simple thermal efficiency parameter (*STEP*) and the production time until the steam to oil ratio (*SOR*) is 8.

Nitrogen Mole Fraction (mol %)	Maximum <i>STEP</i> (Unitless) *	Production Period Until <i>SOR</i> = 8 (Days) *
0 (regular SAGD) †	0.0317 ( <b>0.0312</b> ) ‡	463 (376)
0.1	<b>0.0349</b> ‡ (0.0297)	483 (436)
0.5	0.0334 (0.0247)	487 (429)
1.0	0.0333 (0.0241)	489 (427)
2.0	0.0323 (0.0234)	<b>491</b> ‡ (424)
3.0	0.0307 (0.0232)	477 (429)
5.0	0.0263 (0.0230)	474 (441)
7.0	0.0237 (0.0216)	464 (443)
10.0	0.0218 (0.0184)	451 ( <b>445</b> ) ‡

\* To distinguish the value according to the finite and the infinite aquifer. The format is “the value of the finite case (that of the infinite case)”; † This condition means steam-assisted gravity drainage (SAGD) operation without nitrogen injection; ‡ It represents the maximum value (bold and underlined).

This paper concentrates on the flow characteristics between the top water zone and the steam chamber, i.e., the water influx from the top aquifer and the fluids loss from steam chambers in the homogeneous reservoir. To ensure practical applicability, additional discussions are required, e.g., reservoir heterogeneity, various flow directions in 3D reservoirs, the chamber interferences, and the optimum wellpad system consisting of several wellpairs [4–6]. The reservoir heterogeneity, i.e., the variation of the rock property and the facies models according to the location, should be considered since it is able to influence the flowing characteristics of the displacing fluid, as well as the entire performance [24–27]. An impermeable barrier, e.g., the shale layer that exists in the bitumen deposit, is able to impede the water influx into the steam chamber, while it also interrupts the optimum enlargement of the steam chamber in terms of the energy efficiency. This study assumes the functional relationship of the gas-liquid *K* value as defined in Equation (1) and neglects the gas solubility and the originally-dissolved amount of non-condensable gas in the oil. The experimental validation of thermodynamic data, e.g., the gas solubility and *K* value, would be helpful to explain the accurate flow of gas phases. The regular SAGD produces the non-condensable gas, e.g., methane, and thereby the thermal simulation considered the originally-dissolved non-condensable gas could increase the reliability [14,15,18,28–30]. The non-condensable gas is not viscous, and its density in relation to the diluted fluid mixture is vastly different; therefore, it can release into the aquifer without difficulty and form the flow channel between the thief zone and the steam chamber. An additive that is more viscous and soluble than nitrogen would be a more effective substitute, e.g., polymer, surfactant, or hexane, among others [8,9,31]. Since the thief zone is problematic regarding the difficulty to generate optimal shapes of the steam chamber, fracture-assisted steam technology for the growing of the chamber sideways is one alternative method [32].

#### 4. Conclusions

This paper analyzed the effects of the top water-bearing zone, i.e., aquifer, on the production performance of the SAGP process. Assuming two different aquifers, i.e., finite and infinite cases, the production performance and the gas saturation were observed. The presence of the top water-bearing zone overlying the oil sands deposit can be problematic in terms of the energy efficiency, as well as the oil recovery. The steam loss and the water influx interrupt the growth of the steam chamber. The fixed-size thief zone is more favorable than the infinite case for conducting the SAGP process. The oil sands formation with the finite-sized aquifer produces more oil and less water compared with the case of the infinite aquifer. The amounts of the water influx and the steam loss can be case-sensitive to the boundary definitions. With the increasing mol % of nitrogen, the producing time with energy efficiency increases, but the chamber growth is limited. If the size of the heat thief zone is fixed, the optimum operations of the SAGP process would be available; 0.1 mol % of nitrogen is most effective from the perspective of energy-efficient operations while 2 mol % would be the better option to enlarge

the producible period without significant heat loss in this study. For the infinite aquifer with mass transfer at the boundaries, the continuous water influx and the significant heat loss interrupted the thermal operations.

**Acknowledgments:** This study was supported by Basic Science Research Program through the National Research Foundation of Korea (NRF) funded by the Ministry of Education (2017R1D1A1B04033060) and also by the Korea Institute of Energy Technology Evaluation and Planning (KETEP) and the Ministry of Trade, Industry and Energy (MOTIE), Korea (no. 20172510102150).

**Author Contributions:** Changsoo Lee performed the numerical simulations for SAGP operations. Changhyup Park contributed to the preparation of the whole paper, the model development, and analyzed the results. Soobin Park participated in methodology discussions and the thermal simulations. Authorship must be limited to those who have contributed substantially to the work reported.

**Conflicts of Interest:** The authors declare no conflict of interest.

## References

1. Barillas, J.L.M.; Dutra, T.V., Jr.; Mata, W. Reservoir and operational parameters influence in SAGD process. *J. Petrol. Sci. Eng.* **2006**, *54*, 34–42. [[CrossRef](#)]
2. Shin, H.; Polikar, M. Review of reservoir parameters to optimize SAGD and Fast-SAGD operating conditions. *J. Can. Petrol. Technol.* **2006**, *46*, 35–41. [[CrossRef](#)]
3. Gates, I.D.; Larter, S.R. Energy efficiency and emissions intensity of SAGD. *Fuel* **2014**, *115*, 706–713. [[CrossRef](#)]
4. Park, C.; Yoo, J.; Kang, J.M.; Jang, I.; Lee, C.; Choi, J. Reservoir heterogeneity affecting steam communication between multiple well-pairs for steam assisted gravity drainage. *Energy Explor. Exploit.* **2014**, *32*, 891–903. [[CrossRef](#)]
5. Park, C.; Choi, J.; Lee, C.; Ahn, T.; Jang, I. Operation constraints of steam assisted gravity drainage considering steam interference to accomplish optimum bitumen recovery. In Proceedings of the Twenty-Fifth International Ocean and Polar Engineering Conference, Kona, HI, USA, 21–26 June 2015.
6. Choi, J.; Park, C.; Jang, I. Optimisation of well constraints based on wellpad system to accomplish a successive thermal process in a heterogeneous oil-sands reservoir. *Int. J. Oil Gas Coal Technol.* **2017**, *16*, 27–42. [[CrossRef](#)]
7. Crerar, E.R.; Arnott, R.W.C. Facies distribution and stratigraphic architecture of the lower Cretaceous McMurray formation, Lewis Property, Northeastern Alberta. *Bull. Can. Petrol. Geol.* **2007**, *55*, 99–124. [[CrossRef](#)]
8. Sheng, J.J. *Enhanced Oil Recovery: Field Case Studies*; Gulf Professional Publishing: Oxford, UK, 2013; pp. 413–445, ISBN 978-0-12-386545-8.
9. Zhou, X.; Zeng, F.; Xhang, L. Improving steam-assisted gravity drainage performance in oil sands with a top water zone using polymer injection and the fishbone well pattern. *Fuel* **2016**, *184*, 449–465. [[CrossRef](#)]
10. Law, D.H.S.; Nasr, T.N.; Good, W.K. Field-scale numerical simulation of SAGD process with top-water thief zone. *J. Can. Petrol. Technol.* **2003**, *42*, 32–38. [[CrossRef](#)]
11. Alturki, A.; Gates, I.D.; Maini, B. On SAGD in oil sands reservoirs with no caprock and top water zone. *J. Can. Petrol. Technol.* **2011**, *50*, 21–33. [[CrossRef](#)]
12. Butler, R. The steam and gas push (SAGP). *J. Can. Petrol. Technol.* **1999**, *38*, 54–61. [[CrossRef](#)]
13. Jiang, Q.; Butler, R.; Yee, C.T. The steam and gas push (SAGP)-2: Mechanical analysis and physical model testing. *J. Can. Petrol. Technol.* **2000**, *39*, 52–61. [[CrossRef](#)]
14. Ito, Y.; Ichikawa, M.; Hirata, M. The effect of gas injection on oil recovery during SAGD projects. *J. Can. Petrol. Technol.* **2001**, *40*, 38–43. [[CrossRef](#)]
15. Aherne, A.L.; Birrel, G.E. Observations relating to non-condensable gases in a vapour chamber: Phase B of the Dover Project. In Proceedings of the SPE International Thermal Operations and Heavy Oil Symposium and International Horizontal Well Technology Conference, Calgary, AB, Canada, 4–7 November 2002.
16. Gao, Y.; Liu, S.; Shen, D.; Guo, E.; Bao, Y. Improving oil recovery by adding N<sub>2</sub> in SAGD process for super-heavy crude reservoir with top-water. In Proceedings of the SPE Russian Oil and Gas Technical Conference, Moscow, Russia, 28–30 October 2008.
17. Rios, V.S.; Laboissiere, P.; Trevisan, O.V. Economic evaluation of steam and nitrogen injection on SAGD process. In Proceedings of the SPE Latin American and Caribbean Petroleum Engineering Conference, Lima, Peru, 1–3 December 2010.

18. Al-Murayri, M.T.; Harding, T.G.; Maini, B. Impact of noncondensable gas on performance of steam-assisted gravity drainage. *J. Can. Petrol. Technol.* **2011**, *50*, 46–54. [[CrossRef](#)]
19. Chung, S.; Min, B.; Park, C.; Kang, J.M.; Kam, D. Operation strategy of steam and gas push in the presence of top water thief zone. In Proceedings of the 73rd EAGE Conference and Exhibition Incorporating SPE Europec 2011, Vienna, Austria, 23–26 May 2011.
20. Chung, S.; Kang, J.M.; Park, C. Sensitivity analysis on steam and gas push to reduce heat loss into the top water-bearing area overlaying oil sands. In Proceedings of the Twenty-third International Offshore and Polar Engineering Conference, Anchorage, AK, USA, 30 June–5 July 2013; ISOPE-I-13-198.
21. Doan, L.T.; Harschnitz, B.; Shiga, N.; Pennacchioli, E.; Park, B. NCG co-injection at Hangingstone Demonstration Project: Case study and analysis. In Proceedings of the SPE Heavy Oil Conference, Calgary, AB, Canada, 10–12 June 2014.
22. Computer Modelling Group (CMG). *STARS User Guide*; Computer Modelling Group: Calgary, AB, Canada, 2014; pp. 11–54.
23. Shin, H.; Polikar, M. Simple thermal efficiency parameter as an economic indicator for SAGD performance. In Proceedings of the SPE Hydrocarbon Economics and Evaluation Symposium, Dallas, TX, USA, 3–5 April 2005.
24. Larter, S.; Adams, J.; Gates, I.D.; Bennett, B.; Huang, H. The origin, prediction and impact of oil viscosity heterogeneity on the production characteristics of tar sand and heavy oil reservoirs. *J. Can. Petrol. Technol.* **2006**, *47*, 52–61. [[CrossRef](#)]
25. Kim, H.; Park, C.; Min, B.; Chung, S.; Kang, J.M. Multiphase flow simulation for in situ combustion to investigate field-scale hydraulic heterogeneity and air injection rate affecting oil production. *Energy Source Part A* **2014**, *36*, 2328–2337. [[CrossRef](#)]
26. Lee, H.; Jin, J.; Shin, H.; Choe, J. Efficient prediction of SAGD productions using static factor clustering. *J. Energy Resour. Technol.* **2015**, *137*, 032907. [[CrossRef](#)]
27. Lajevardi, S.; Babak, O.; Deutsch, C.V. Estimating barrier shale extent and optimizing well placement in heavy oil reservoirs. *Petrol. Geosci.* **2015**, *21*, 322–332. [[CrossRef](#)]
28. Al-Murayri, M.; Harding, T.G.; Maini, B.B. Solubility of methane, nitrogen, and carbon dioxide in bitumen and water for SAGD modelling. *J. Can. Petrol. Technol.* **2011**, *50*, 34–45. [[CrossRef](#)]
29. Varet, G.; Montel, F.; Nasri, D.; Daridon, J. Gas solubility measurement in heavy oil and extra heavy oil at vapor extraction (VAPEX) conditions. *Energy Fuels* **2013**, *27*, 2528–2535. [[CrossRef](#)]
30. Haddadnia, A.; Zirrahi, M.; Hassanzadeh, H.; Abedi, J. Solubility and thermos-physical properties measurement of CO<sub>2</sub>- and N<sub>2</sub>-Athabasca bitumen systems. *J. Petrol. Sci. Eng.* **2017**, *154*, 277–283. [[CrossRef](#)]
31. Kam, D.; Park, C.; Min, B.; Kang, J.M. An optimal operation strategy of injection pressures in solvent-aided thermal recovery for viscous oil in sedimentary reservoirs. *Petrol. Sci. Technol.* **2013**, *31*, 2378–2387. [[CrossRef](#)]
32. Speight, J.G. *Introduction to Enhanced Recovery Methods for Heavy Oil and Tar Sands*; Gulf Professional Publishing: Oxford, UK, 2016; Chapter 9; ISBN 978-0-12-849906-1.

